

Out-of-plane ferroelectricity, magnetoelectric coupling and persistent spin texture in two-dimensional multiferroics

Ying Zhou,^{1,*} Cheng-Ao Ji,^{1,*} Shuai Dong,¹ and Xuezheng Lu^{1,†}

¹*Key Laboratory of Quantum Materials and Devices of Ministry of Education, School of Physics, Southeast University, Nanjing 211189, China*

Two-dimensional multiferroics with out-of-plane ferroelectricity hold significant promise for miniaturized magnetoelectric spin-orbit transistors, yet systems combining robust ferroelectricity and strong magnetoelectric coupling are exceedingly rare. Here, we demonstrate that epitaxial strain stabilizes out-of-plane ferroelectricity in exfoliated two-dimensional Ruddlesden-Popper derivatives. The hybrid improper ferroelectric Pc phase transitions to a competing $P2_1$ phase with purely in-plane polarization upon switching, accompanied by a 90° rotation of weak ferromagnetism. Crucially, the Pc phase exhibits altermagnetism, while $P2_1$ displays full-Brillouin-zone band splitting, with persistent spin textures rotating 90° at the phase boundary. This work establishes a pathway to engineer two-dimensional multiferroics that integrate vertical polarization, magnetoelectric coupling, and switchable spin textures—key features for next-generation spintronic devices.

I. INTRODUCTION

Ferroelectric materials have attracted considerable attention for modern technologies due to their bistable polarization states, making them promising candidates for nonvolatile memory applications [1–3]. The demand for miniaturized devices requires stabilization of out-of-plane ferroelectricity (i.e., oriented along the thin-film growth direction), thus, their associated functionalities such as multiferroicity, magnetoelectricity and ferroelectric switchable spin texture can persist as the film thickness decreases [4, 5]. Nevertheless, conventional ferroelectrics possess an intrinsic critical thickness below which the out-of-plane polarization disappears, fundamentally restricting their implementation in ultrathin devices [6, 7].

Recently, the study of two-dimensional (2D) materials has found promising mechanisms for exploring out-of-plane ferroelectricity in the ultrathin film and some of them have been realized in experiments [8–10]. For instance, 2D CuInP_2S_6 was experimentally confirmed to host vertical ferroelectricity, driven by the displacement of Cu and In ions along the crystallographic c -axis, representing the first confirmed 2D system with intrinsic out-of-plane polarization [11, 12]. First principles calculations subsequently revealed that interlayer sliding in the materials with van der Waals (vdW) bilayers (e.g., BN, AlN, ZnO, MoS_2 , GaSe, etc.) can lead to vertical polarization [13]. Experimentally, spontaneous out-of-plane polarization has been observed in multi-layer WTe_2 (2–3 layers) [14]. Additionally, 2D $\alpha\text{-In}_2\text{Se}_3$ has been predicted to possess coupled in-plane and out-of-plane polarizations arising from Se atomic displacements [15, 16].

So far, the exploration of 2D materials has largely centered on vdW systems, with very few examples exhibiting both robust out-of-plane ferroelectricity and magne-

toelectric (ME) coupling. In contrast, 3D multiferroics with strong ME coupling typically rely on interconnected transition-metal coordination geometries—such as edge-, corner-, or face-sharing octahedra, tetrahedra, or square pyramids [17–20]. This structural connectivity, while enabling strong ME effects in 3D systems, poses a significant challenge for reducing these materials to their 2D limit, as ultrathin films often lose their out-of-plane ferroelectric properties. However, the experimental breakthroughs in synthesizing 2D monolayers from both layered and nonlayered transition-metal oxides have opened new avenues for investigating ferroelectricity in atomically thin systems [21–24]. Capitalizing on these advances, there is growing interest in leveraging the dense transition-metal networks found in 3D perovskite oxides to engineer 2D materials that retain both out-of-plane ferroelectricity and ME coupling—a critical step toward realizing functional ultrathin multiferroics.

In this work, by using first-principles calculations and group theory analysis, we demonstrate that the structure containing two perovskite layers derived from the quasi-2D Ruddlesden-Popper (RP) $\text{Ca}_3\text{Mn}_2\text{O}_7$ can have out-of-plane ferroelectricity under the epitaxial strain $x \neq y$ (x, y : the in-plane lattice parameters). The stabilized polar phase has the Pc symmetry and the ferroelectricity emerges from the cooperative octahedral rotations and tilts, thus, is the hybrid improper ferroelectricity. Additionally, we predict a phase transition from the Pc to $P2_1$ under the epitaxial strain, where the $P2_1$ phase has the close energy to the Pc phase. Meanwhile, there is a change on the direction of the weak ferromagnetism (wFM) at the phase transition. More interestingly, the Pc phase has the altermagnetic ordering and $P2_1$ phase has a full-Brillouin-zone (FBZ) band splitting. Both phases have the persistent spin textures (PST) that can be transformed to each other through changing the out-of-plane hybrid improper ferroelectricity (OP-HIF). In our studied PST, the quadratic terms of the momentum vectors dominate the spin-orbit field, contrasting to the previously reported PST with the linear or cubic terms

* These authors contributed equally to this work

† xuezhenglu@seu.edu.cn

of the momentum vectors, and a 90° rotation of the PST can occur at phase transition. Moreover, we also find the Pc phase in the RP halides, where the epitaxial strain stabilizes the Pc phase. These results establish the design principles for discovering materials with out-of-plane ferroelectricity and strong ME coupling based on the perovskite structures.

II. COMPUTATIONAL METHODS

The first-principles calculations based on density functional theory (DFT) were performed using the projector-augmented wave method, as implemented in the Vienna *ab initio* simulation package [25–27]. The Perdew-Burke-Ernzerhof functional was used as the exchange-correlation functional [28, 29]. A vacuum space of 25 Å was added to avoid interaction between neighboring periodic images. We used a cutoff energy of 600 eV for the plane-wave bases, and a Γ -centered $5 \times 5 \times 1$ k -point mesh for the Brillouin zone integration. The in-plane lattice constants and internal atomic coordinates of each structural phase were relaxed until the Hellman-Feynman force on each atom is less than 0.005 eV/Å. A convergence threshold of 10^{-6} eV was used for the electronic self-consistency loop. To describe correlated $3d$ electrons of Mn, the GGA+ U method is applied [30], and the U_{eff} are 3.5 eV and 6 eV for 2D $\text{Ca}_3\text{Mn}_2\text{O}_7$ and 2D $\text{KAg}_2\text{Mn}_2\text{Cl}_7$, respectively. Phonon band structures were calculated using density functional perturbation theory (DFPT). The phonon frequencies and corresponding eigen-modes were calculated on the basis of the extracted force-constant matrices with a $4 \times 4 \times 1$ supercell, as implemented in the PHONOPY code [31]. The polarization was calculated by using the Berry phase method [32]. The energy barrier of different ferroelectric switching paths was determined by using the climbing nudged elastic band method [33]. The ISOTROPY tool [34] was used to help with the group-theoretical analysis.

III. RESULTS AND DISCUSSION

In bulk $\text{Ca}_3\text{Mn}_2\text{O}_7$, first-principles calculations predicted the existence of hybrid improper ferroelectricity, in which the polarization is driven by a trilinear coupling interaction (PQ_RQ_T) among the polarization (P), in-phase octahedral rotation (Q_R) and out-of-phase tilt (Q_T) [35]. Without this anharmonic mode-mode interaction, polarization cannot be condensed by itself. Through the trilinear coupling interaction, a ME coupling mechanism was elucidated within the G-type antiferromagnetic (AFM) structure, where the wFM is induced by the Dzyaloshinskii-Moriya (DM) interaction that is proportional to Q_T , thus, a simultaneous change of polarization and Q_T can lead to a switchable wFM. But if another polarization switching through a simultaneous change of P and Q_R occurs, there is no control of the wFM. In fact,

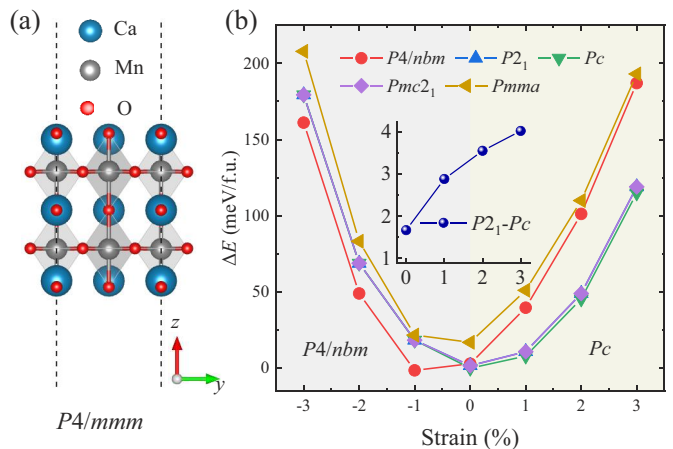


FIG. 1. (a) The high-symmetry $P4/mmm$ structure of the 2D-RP structure of $\text{Ca}_3\text{Mn}_2\text{O}_7$. (b) The energies of several 2D-RP structures of $\text{Ca}_3\text{Mn}_2\text{O}_7$ as a function of the epitaxial strain. The energies are calculated with respect to that of $P4/nbm$ at -1% strain. The insert shows the energy differences of the $P2_1$ phase relative to the Pc phase as a function of the tensile strain ranging from 0% - 3%.

these two polarization switching paths usually compete with each other, which leads to the ME coupling remaining unrealized in experiments so far. This is a dilemma that most type-I multiferroics encounter. For example, BiFeO_3 also has two polarization switching paths [36, 37]. In one path, there is only change of polarization and out-of-phase rotations around the pseudocubic [111] direction cannot be changed. In another path, both polarization and out-of-phase rotations can be switched. Only the latter one can have simultaneous change of wFM and polarization [38–43].

Although many studies reported the layered oxides with the polar ground state phase such as in the RP phase, Aurivillius phase, Dion-Jacobson phase, the realization of ME couplings in these materials in experiments are still difficult as mentioned above. To address the above dilemma, the investigations on the RP halides provided insight into the solutions: (1) searching for the polar ground state phase with low symmetry. For example, the Pc phase can be stabilized in $\text{KAg}_2\text{Mn}_2\text{Cl}_7$ with G-type AFM ordering [44], where both Q_R and Q_T can control the wFM because that the only one mirror symmetry cannot lead to a perfect cancellation of the weak antiferromagnetism controlled by Q_R . Moreover, the Pc phase of $\text{KAg}_2\text{Mn}_2\text{Cl}_7$ has the OP-HIF, which is the secondary mode and induced by two out-of-phase (Q_{R1}) and in-phase (Q_{R2}) octahedral rotations, i.e., $PQ_{R1}Q_{R2}$. Then, the switching of the OP-HIF can lead to a change of either Q_{R1} or Q_{R2} . No matter which one is changed, the simultaneous change of the OP-HIF and wFM can occur. This is not related to the polarization switching processes. (2) Finding reliable polar-to-nonpolar phase transition with the simultaneous change of the polarization and magnetism, which was found in $(\text{Rb},\text{K})_3\text{Mn}_2\text{Cl}_7$

with G-type AFM ordering and there are two kinds of Q_T in the two phases that result in the different directions of wFM. Unfortunately, the polar-to-nonpolar phase transition with the simultaneous change of the polarization and magnetism in $(\text{Rb,K})_3\text{Mn}_2\text{Cl}_7$ was only realized by varying the temperature, that is, thermally controlled ME coupling [45].

It is interesting to continue searching the ME multiferroics, especially, one has out-of-plane ferroelectricity, below 1 nanometer in the RP materials. Previous study showed that the double-perovskite-layer structure derived from $\text{Ca}_3\text{Mn}_2\text{O}_7$ can have a $Pmc2_1$ polar ground state structure with the in-plane polarization and G-type AFM orderings under biaxial strain [46]. Although the ME coupling was also predicted in the 2D structure, that still relied on the trilinear coupling interaction, thus, may be invalid when the polarization switching through the change of Q_R occurs. Our DFT calculations indicate that the Pc phase found in the RP halides can be stabilized in the double-perovskite-layer structure (hereafter, it is called 2D-RP structure) derived from $\text{Ca}_3\text{Mn}_2\text{O}_7$ by the epitaxial strain with $x = 1.004y$ (see Fig. 1 and Fig. S1 in the Supplemental Material [47]). The form of the epitaxial strain in our study may be a reasonable description of a strained film for some materials where a buffer layer usually exists between film and substrate, resulting in imperfect registry [48]. Under tensile strain, the energy difference between the metastable $P2_1$ and Pc phases increases from approximately 1.5 to 4.5 meV/f.u. as the strain rises from 0% to 3%, as shown in Fig. 1 (b). And the previously found $Pmc2_1$ phase becomes $P2_1$ phase with the epitaxial tensile strain. The energy difference between Pc and $P2_1$ phases can become large with increasing the x/y ratio (e.g., 11 meV/f.u. at 1% strain and $x = 1.04y$). Therefore, the x/y ratio may be an effective factor to engineer the out-of-plane ferroelectricity in the 2D-RP structure. We also find the Pc ground state phase in the 2D-RP structure of the RP halides (see Fig. S2, Fig. S3 and Table S3 [47]).

Next, the mode decomposition was performed for Pc phase with respect to high-symmetry $P4/mmm$ phase [see Fig. 1 (a)]. As shown in Fig. 2(a), there are six main phonon modes, which are an in-plane polar mode having irreducible representation (irrep) Γ_5^- , an out-of-plane polar mode Γ_3^- , an antiferroelectric (AFE) mode Γ_5^+ , an in-phase octahedral rotational (OOR_i) mode M_2^+ around z direction, an out-of-phase octahedral rotational (OOR_o) mode M_4^- around z direction and an out-of-phase octahedral tilt (OOT) mode M_5^- around x direction. Then, two trilinear coupling interactions can be obtained, which are $Q_{\Gamma_5^-}Q_{M_2^+}Q_{M_5^-}$ and $Q_{\Gamma_3^-}Q_{M_2^+}Q_{M_4^-}$. Since only the OOR_i and OOT have large energy gain [see Fig. 2(b)], the in-plane and out-of-plane polarizations are induced by the trilinear coupling interactions $Q_{\Gamma_5^-}Q_{M_2^+}Q_{M_5^-}$ and $Q_{\Gamma_3^-}Q_{M_2^+}Q_{M_4^-}$, respectively. Because the OP-HIF has the ability to overcome the depolarized field [44, 49], thus the Pc phase can be stable in the 2D-RP structure. But the depolarized field still have effects on the OP-HIF,

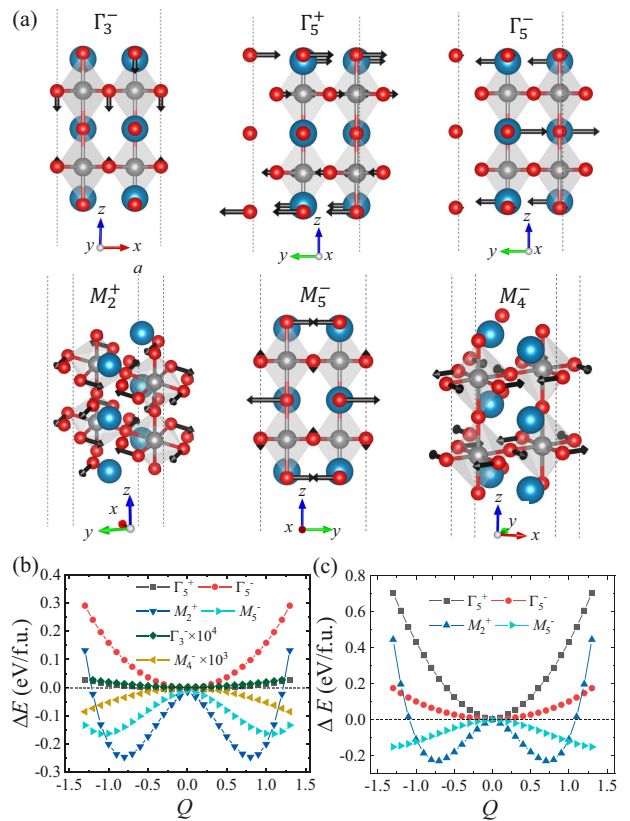


FIG. 2. (a) The main atomic displacement patterns in the Pc phase of the 2D-RP structure of $\text{Ca}_3\text{Mn}_2\text{O}_7$, represented by the designated irreps of the $P4/mmm$ phase. (b) Shows the energy of each atomic displacement shown in the high-symmetry $P4/mmm$ phase where the mode amplitude Q is scaled by the original amplitude of the corresponding atomic displacement in the Pc structure. The energy is computed relative to the high-symmetry $P4/mmm$ phase. Energy gains for the M_4^- and Γ_3^- modes are magnified by the factors of 10^3 and 10^4 , respectively.

(c) The energy of each atomic displacement in the $P2_1$ phase versus the mode amplitude Q .

where the remanent polarization with the existence of the depolarized field will be small in the ultrathin film [50]. The computed polarization of the Pc phase in the 2D-RP structure is $(11.03, 0, 0.14) \mu\text{C}/\text{cm}^2$, in which the in-plane hybrid improper ferroelectricity (IP-HIF) is comparable to the other RP materials in bulk [40, 51]. In the $P2_1$ phase, there are four main phonon modes, which are Γ_5^- , Γ_5^+ , M_2^+ and M_5^- [see Fig. 2(c) and Table S2 [47]]. The $M_5^-(0, a)$ has different order parameter directions (OPDs) from $M_5^-(a, 0)$ of Pc phase and the $P2_1$ phase only has IP-HIF $(0, 10.28, 0) \mu\text{C}/\text{cm}^2$ that arises from $Q_{\Gamma_5^-}Q_{M_2^+}Q_{M_5^-}$.

In our nudged elastic band (NEB) calculations [33] [see Fig. 3 (c)], we find that the IP-HIF can be switchable with a barrier of 40 meV/f.u., while the switching barrier is 120 meV/f.u. for OP-HIF indicating that it may be hard to be switchable. In our two-step polarization

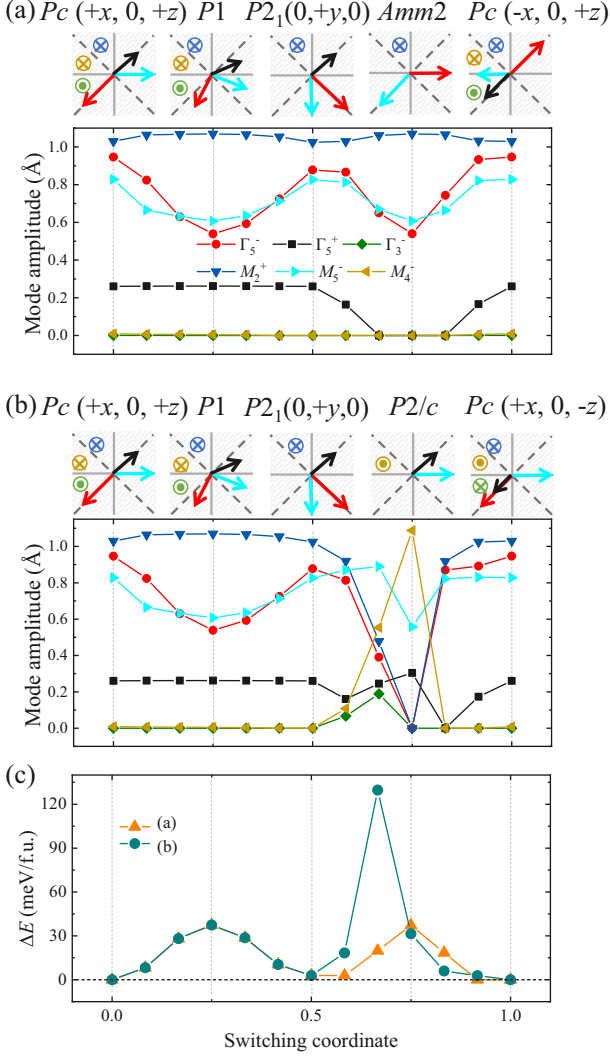


FIG. 3. Ferroelectric switching paths with the switched (a) the IP-HIF and the OP-HIF (b) of the Pc for 2D-RP structure of $\text{Ca}_3\text{Mn}_2\text{O}_7$ at 1% tensile strain, where x , y , and z denote the polarization components along the three Cartesian axes. Symbols in upper panels indicate the evolution of order parameters during polarization switching: arrows for 2D order parameters (Γ_5^+ [black], Γ_5^- [red], M_5^- [cyan]); \otimes/\odot for 1D order parameters (Γ_3^- [green], M_2^+ [blue], M_4^- [gold]). The bottom part shows the absolute amplitudes as a function of the switching coordinate, obtained from nudged elastic band calculations. (c) The computed energy barriers for the paths shown in (a)–(b).

switching paths, the Pc phase may be transformed to the $P2_1$ phase by tuning the OP-HIF by applying out-of-plane electric field, where our computed barrier of 40 meV/f.u. and OP-HIF of $0.14 \mu\text{C}/\text{cm}^2$ are comparable to those in the vdW materials [52, 53]. The 90° twin domains of the Pc and $P2_1$ phases are also considered in the polarization switching, as it usually leads to a low energy barrier [40, 45]. We find that the Pc with IP-HIF along y direction and OP-HIF (twin domain of Pc) and

$P2_1$ with IP-HIF along x direction (twin domain of $P2_1$) cannot exist with $x = 1.004y$, since the twin domain of Pc and twin domain of $P2_1$ are unstable and will be relaxed to $P2_1$ and Pc , respectively. Thus, the slightly anisotropic x and y under epitaxial strain will help the transformation between the $P2_1$ with IP-HIF along the y direction and Pc with the IP-HIF along the x direction by tuning the OP-HIF. Besides, the Pc -to- $P2_1$ transition can also be accessible through low in-plane electric field as the IP-HIF is $11.03 \mu\text{C}/\text{cm}^2$.

Then, we consider the modes changes in the ferroelectric switching paths [40–43]. In the first path shown in Fig. 3(a), the initial Pc phase exhibits the polarization along $(+x, 0, +z)$. This state evolves through an intermediate $P2_1$ phase with the polarization along $(0, +y, 0)$, finally reaching the Pc phase with the polarization along $(-x, 0, +z)$ station. In this path, the M_2^- rotational mode is kept and the Γ_5^- polar mode and M_5^- tilt mode are switched, which is consistent with the existence of the trilinear coupling $\sim Q_{\Gamma_5^-} Q_{M_2^+} Q_{M_5^-}$. In the second ferroelectric reversal path shown in Fig. 3(b), the Pc phase has the switched polarization polarized along $(+x, 0, -z)$. Along this switching path, the Γ_3^- polar mode and M_4^- mode are changed and the M_2^+ is still kept, which again fulfills the trilinear coupling interaction of $Q_{\Gamma_3^-} Q_{M_2^+} Q_{M_4^-}$. In both switching paths, the M_2^+ rotational mode is unchanged because of its large energy gain in stabilizing the ground state Pc phase, and this can facilitate the switching processing with the low energy barrier.

Next, we focus on the magnetic properties. The magnetic structure of Mn_4^+ ions has G-type magnetic ordering for the main spin direction, which has been demonstrated in both the 2D-RP with the biaxial strain ($x = y$) and bulk $\text{Ca}_3\text{Mn}_2\text{O}_7$ structures [46, 54–57]. Our DFT+ U +SOC (spin-orbital coupling) calculations show that the magnetocrystalline anisotropy energy (MAE) is along the out-of-plane direction for the Pc and $P2_1$ phases, as shown in Fig. S4 [47]. The wFM are computed to $(0.001, 0.038, 0.000)\mu_B/\text{u.c.}$ and $(0.042, 0.002, 0.000)\mu_B/\text{u.c.}$ for the Pc and $P2_1$ phases, respectively, where each unit cell (u.c.) contains four magnetic atoms. The computed magnetic configurations by including SOC are consistent with the symmetry-adapted configurations of (G, FM, G) for the Pc phase (the magnetic point groups (MPG) is m) and (FM, A, G) for the $P2_1$ phase (the MPG is $2'$), as shown in Fig. 4(a).

By symmetry analysis [58], we discovered that the spin up and spin down sublattices are connected by the spin space symmetry $[C_2||\{m_y|\tau\}]$ and there are no inversion and translational symmetries between the antiparallel spins in Pc phase [see Fig. 4 (b)]. Hence, we can confirm that the G-type AFM of Pc phase is altermagnetic, consistent with our band structure calculations without SOC [see Fig. 4 (c)].

The band splitting of Pc phase without SOC between the spin-up and spin-down bands near the N point

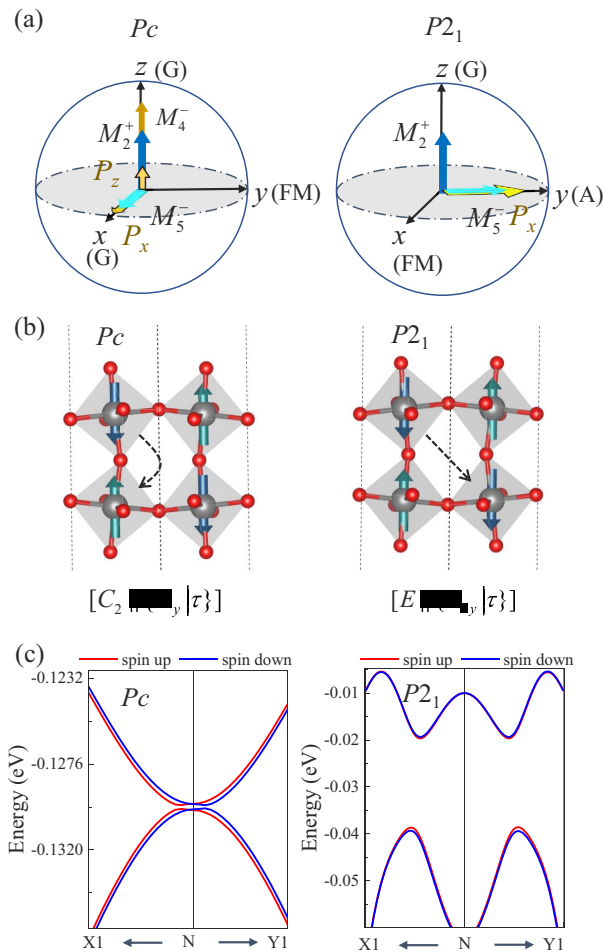


FIG. 4. (a) Magnetic symmetry analysis for the initial P_c ($+x, 0, +z$) and the intermediate P_{2_1} ($0, +y, 0$) phases. In the P_c phase, the magnetic configurations along the three orthogonal axes are: G-type AFM along the x -axis, FM along the y -axis, and G-type AFM along the z -axis. In the P_{2_1} phase, the configurations correspond to (FM, A-type AFM, G-type AFM) along the three axes. Blue/golden arrows denote the in-phase (M_2^+)/out-of-phase (M_4^-) rotation mode, cyan arrows represent the tilt mode (M_5^-), and yellow arrows indicate the direction of the polarization. (b) Spin ordering with the antiparallel/parallel spins mapped by the spin group operations for P_c and P_{2_1} phases. (c) The band structures without SOC of the P_c and P_{2_1} phases at 1% strain, the VBM is set to 0 eV. The kpoints are N (0.5, 0, 0), X1 (0.2, 0.2, 0), Y1 (0.2, -0.2, 0).

shown in Fig. 4 (c) is about 0.18 meV. By considering the SOC, the band splitting becomes 0.20 meV. Although the band splitting is small, the variation of the band splitting with the momentum vector k ($\sim \Delta E / \Delta k$, $\Delta E = E_{\text{spin-up}} - E_{\text{spin-down}}$) with and without SOC are about $22.16 \text{ meV}\cdot\text{\AA}$ and $20.68 \text{ meV}\cdot\text{\AA}$ in the P_c phase. This band splitting strength $\sim \Delta E / \Delta k$ is comparable to those in the quantum-wells or $\text{LaAlO}_3/\text{SrTiO}_3$ heterointerfaces that typically exhibit $1 - 10 \text{ meV}\cdot\text{\AA}$ [59–61]. These systems have been extensively studied for their spin tex-

tures in experiments. Furthermore, recent experimental advances have already demonstrated the observation of the altermagnetic phases in the materials such as $\alpha\text{-MnTe}$ and RuO_2 , using techniques like angle-resolved photoemission spectroscopy (ARPES) and magnetic circular dichroism [62, 63]. These results confirm that altermagnetism can be achieved and detected in real systems, indicating strong potential for experimental realization in other candidate materials as well.

For the P_{2_1} phase, there is no any symmetry between the antiparallel spins and the parallel spins are connected by the symmetry $[E \parallel \{C_{2y} | \tau\}]$ [see Fig. 4 (b)], therefore, the P_{2_1} should have FBZ band splitting without SOC. This is demonstrated in our band structure calculations without SOC [see Fig. 4 (c)]. To make the FBZ band splitting large in the P_{2_1} phase, an electric field (E) of $0.25 \text{ V}/\text{\AA}$ is applied to be along the 2-fold rotation in which the P_{2_1} symmetry is kept, following a method based on a Landau model originally used to compute the linear ME response [64]. Then, a more visible FBZ band splitting can be obtained [see Fig. 5(b)]. If the electric field is applied to be perpendicular to the mirror plane in the P_c phase, there will be no symmetry among antiparallel spins and the FBZ band splitting without SOC can also be observed [see Fig. 5(a)]. Besides, the FBZ band splitting without SOC can be tuned by the OP-HIF through the P_c -to- P_{2_1} phase transition, leading to a change on the amplitude of FBZ band splitting around conduction band maximum (CBM) that can be related to the carrier/spin transport properties [65, 66]. In the P_c phase, the effective mass around the CBM is $1.8m_0$ (electron mass) along the Γ -Y direction, while in the P_{2_1} phase, it reduces to $0.7m_0$ along Γ -X (see Fig. S8 [47]). Our findings take advantages over the previous studies by asymmetric ion substitution in bulk or in the other 2D materials where the full-Brillouin-zone band splitting cannot be tunable [67, 68].

Previous theory combined with experiment has demonstrated the existence of quadratic spin texture that is unique to altermagnetic materials [69] and the ferroelectric control of the spin texture is of great interest. Considering the altermagnetic ordering and ferrimagnetic ordering in the P_c and P_{2_1} phases where the \mathcal{T} is absent, we further calculate the band structure and spin texture including SOC effect. Our band calculations show that the CBM is located in Γ in both phases (P_c and P_{2_1}) with the band splitting around 12 meV and 6 meV, respectively. Interestingly, as is presented in Figs. 5(c) and (d), PST is discovered around CBM in both phases.

Given the MPG of P_c and P_{2_1} phases (i.e. m and $2'$), the $\mathbf{k} \cdot \mathbf{p}$ Hamiltonian around CBM in P_c and P_{2_1} phases can be constructed according to the magnetic collittle group of Γ , that is, m and $2'$. In the $k_x - k_y$ plane in the P_c phase, the Hamiltonian derived from the $\mathbf{k} \cdot \mathbf{p}$ theory around Γ with m_y symmetry is:

$$H = \sigma_x \alpha_1 k_x k_y + \sigma_y (\beta_1 k_x^2 + \beta_2 k_y^2) + \sigma_z \gamma_1 k_x k_y \quad (1)$$

It is obvious that the spin texture around Γ is dominated

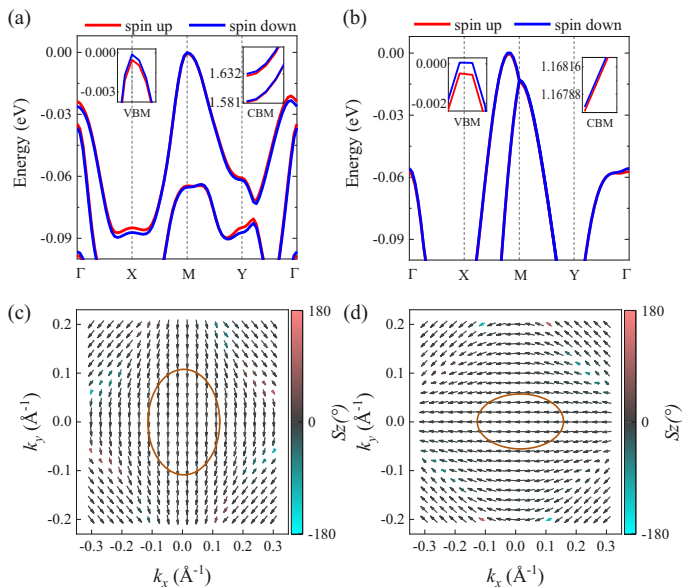


FIG. 5. (a) and (b) show the band structures without SOC of the Pc and $P2_1$ phases at 1% strain with an applied electric field of 0.25 V/\AA , the VBM is set to 0 eV . (c) and (d) The PST in the two phases at 1% strain of the 2D-RP structure of $\text{Ca}_3\text{Mn}_2\text{O}_7$ with SOC at $E = 0 \text{ V/\AA}$. The red circle labels the maximum regions of PST (where the spin deviation is less than 5°) when the energy gradient is considered.

by the quadratic term $\sigma_y(\beta_1 k_x^2 + \beta_2 k_y^2)$, giving rise to the PST along y direction presented in Fig. 5(c), which is in accordance with the direction of wFM. According to the Hamiltonian, the direction of S_x will be reversed as the sign of k_x or k_y changes, which is consistent with our DFT calculation. Besides, the component S_z around Γ within the region of PST is negligible.

For the $P2_1$ phase, the Hamiltonian around Γ with \mathcal{TC}_{2y} symmetry is:

$$H = \sigma_x(\alpha_1 k_x^2 + \alpha_2 k_y^2) + \sigma_y \beta_1 k_x k_y + \sigma_z(\gamma_1 k_x^2 + \gamma_2 k_y^2) \quad (2)$$

Similarly, as shown in Fig. 5(d), the quadratic term

$\sigma_x(\alpha_1 k_x^2 + \alpha_2 k_y^2)$ dominate the PST along x direction and the direction of S_y will be reversed as the sign of k_x or k_y changes, which is in agreement with our DFT calculation. Also, the component S_z around Γ within the region of PST is negligible. Due to the difference of dominated quadratic terms enforced by symmetry in the Pc and $P2_1$ phase, the direction of PST along y can be changed to be x direction through the Pc -to- $P2_1$ phase transition by changing OP-HIF.

IV. CONCLUSION

In summary, the epitaxial strain engineering with $a \neq b$ can be used to create the out-of-plane ferroelectricity in the 2D-RP structure. Besides, in the 2D-RP structure of $\text{Ca}_3\text{Mn}_2\text{O}_7$, the out-of-plane ferroelectricity can be tuned to favor a transition into a polar phase with only in-plane ferroelectricity, where there is a change of the direction of wFM that is constrained by the epitaxial strain. Our study facilitates discovery of PST allowing for the long spin lifetime in the materials without \mathcal{T} , which is in contrast to the previously studied PST in the system with the \mathcal{T} or $\tau\mathcal{T}$ symmetry [70–73]. Furthermore, a novel approach is proposed to tune the direction of PST by manipulating out-of-plane ferroelectricity in 2D materials.

ACKNOWLEDGMENTS

Y.Z., C.A.J. and X.-Z.L. were supported by the National Natural Science Foundation of China (NSFC) under Grant No. 12474081, the open research fund of Key Laboratory of Quantum Materials and Devices (Southeast University), Ministry of Education, the Start-up Research Fund of Southeast University. Y.Z. was supported by the SEU Innovation Capability Enhancement Plan for Doctoral Students (Grant No. CXJH_SEU 25135). DFT calculations were performed through the high-performance computers, supported by the Big Data Computing Center of Southeast University.

[1] K. Chang, J. Liu, H. Lin, N. Wang, K. Zhao, A. Zhang, F. Jin, Y. Zhong, X. Hu, W. Duan, Q. Zhang, L. Fu, Q.-K. Xue, X. Chen, and S.-H. Ji, Discovery of robust in-plane ferroelectricity in atomic-thick SnTe, *Science* **353**, 274 (2016).
 [2] S. Dong, H. Xiang, and E. Dagotto, Magnetoelectricity in multiferroics: a theoretical perspective, *Natl. Sci. Rev.* **6**, 629 (2019).
 [3] W. Banerjee, A. Kashir, and S. Kamba, Hafnium oxide (HfO_2) - a multifunctional oxide: A review on the prospect and challenges of hafnium oxide in resistive switching and ferroelectric memories, *Small* **18**, 2107575 (2022).

[4] M. Dawber, K. Rabe, and J. Scott, Physics of thin-film ferroelectric oxides, *Rev. Mod. Phys.* **77**, 1083 (2005).
 [5] J. F. Scott, Applications of modern ferroelectrics, *Science* **315**, 954 (2007).
 [6] J. Junquera and P. Ghosez, Critical thickness for ferroelectricity in perovskite ultrathin films, *Nature* **422**, 506 (2003).
 [7] N. Spaldin, Fundamental size limits in ferroelectricity, *Science* **304**, 1606 (2004).
 [8] Q. Song, C. A. Occhialini, E. Ergecen, B. Ilyas, D. Amoroso, P. Barone, J. Kapeghian, K. Watanabe, T. Taniguchi, A. S. Botana, S. Picozzi, N. Gedik, and R. Comin, Evidence for a single-layer van der Waals mul-

- tiferroic, *Nature* **602**, 601 (2022).
- [9] K. Yasuda, X. Wang, K. Watanabe, T. Taniguchi, and P. Jarillo-Herrero, Stacking-engineered ferroelectricity in bilayer boron nitride, *Science* **372**, 1458 (2021).
- [10] C. Liu, W. Ren, and S. Picozzi, Spin-chirality-driven multiferroicity in van der waals monolayers, *Phys. Rev. Lett.* **132**, 086802 (2024).
- [11] A. Belianinov, Q. He, A. Dziazgys, P. Maksymovych, E. Eliseev, A. Borisevich, A. Morozovska, J. Banys, Y. Vysochanskii, and S. V. Kalinin, CuInP_2S_6 room temperature layered ferroelectric, *Nano Lett.* **15**, 3808 (2015).
- [12] F. Liu, L. You, K. L. Seyler, X. Li, P. Yu, J. Lin, X. Wang, J. Zhou, H. Wang, H. He, S. T. Pantelides, W. Zhou, P. Sharma, X. Xu, P. M. Ajayan, J. Wang, and Z. Liu, Room-temperature ferroelectricity in CuInP_2S_6 ultrathin flakes, *Nat. Commun.* **7**, 12357 (2016).
- [13] L. Li and M. Wu, Binary compound bilayer and multilayer with vertical polarizations: Two-dimensional ferroelectrics, multiferroics, and nanogenerators, *Acs Nano* **11**, 6382 (2017).
- [14] Z. Fei, W. Zhao, T. A. Palomaki, B. Sun, M. K. Miller, Z. Zhao, J. Yan, X. Xu, and D. H. Cobden, Ferroelectric switching of a two-dimensional metal, *Nature* **560**, 336 (2018).
- [15] W. Ding, J. Zhu, Z. Wang, Y. Gao, D. Xiao, Y. Gu, Z. Zhang, and W. Zhu, Prediction of intrinsic two-dimensional ferroelectrics in In_2Se_3 and other $\text{III}_2\text{-VI}_3$ van der waals materials, *Nat. Commun.* **8**, 14956 (2017).
- [16] Y. Zhou, D. Wu, Y. Zhu, Y. Cho, Q. He, X. Yang, K. Herrera, Z. Chu, Y. Han, M. C. Downer, H. Peng, and K. Lai, Out-of-plane piezoelectricity and ferroelectricity in layered $\alpha\text{-In}_2\text{Se}_3$ nanoflakes, *Nano Lett.* **17**, 5508 (2017).
- [17] T. Hu and E. Kan, Progress and prospects in low-dimensional multiferroic materials, *Wires. Comput. Mol. Sci.* **9**, e1409 (2019).
- [18] N. A. Spaldin and R. Ramesh, Advances in magnetoelectric multiferroics, *Nat. Mater.* **18**, 203 (2019).
- [19] N. A. Spaldin, Multiferroics: Past, present, and future, *Mrs Bull.* **42**, 385 (2017).
- [20] S. Dong, J.-M. Liu, S.-W. Cheong, and Z. Ren, Multiferroic materials and magnetoelectric physics: symmetry, entanglement, excitation, and topology, *Adv. Phys.* **64**, 519 (2015).
- [21] V. Nicolosi, M. Chhowalla, M. G. Kanatzidis, M. S. Strano, and J. N. Coleman, Liquid exfoliation of layered materials, *Science* **340**, 1420 (2013).
- [22] J. N. Coleman, M. Lotya, A. O'Neill, S. D. Bergin, P. J. King, U. Khan, K. Young, A. Gaucher, S. De, R. J. Smith, I. V. Shvets, S. K. Arora, G. Stanton, H.-Y. Kim, K. Lee, G. T. Kim, G. S. Duesberg, T. Hallam, J. J. Boland, J. J. Wang, J. F. Donegan, J. C. Grunlan, G. Moriarty, A. Shmeliov, R. J. Nicholls, J. M. Perkins, E. M. Grievson, K. Theuwissen, D. W. McComb, P. D. Nellist, and V. Nicolosi, Two-dimensional nanosheets produced by liquid exfoliation of layered materials, *Science* **331**, 568 (2011).
- [23] A. P. Balan, S. Radhakrishnan, C. F. Woellner, S. K. Sinha, L. Deng, C. de los Reyes, B. M. Rao, M. Paulose, R. Neupane, A. Apte, V. Kochat, R. Vajtai, A. R. Harutyunyan, C.-W. Chu, G. Costin, D. S. Galvao, A. A. Marti, P. A. van Aken, O. K. Varghese, C. S. Tiwary, A. M. M. R. Iyer, and P. M. Ajayan, Exfoliation of a non-van der waals material from iron ore hematite, *Nat. Nanotechnol.* **13**, 602 (2018).
- [24] D. Ji, S. Cai, T. R. Paudel, H. Sun, C. Zhang, L. Han, Y. Wei, Y. Zang, M. Gu, Y. Zhang, W. Gao, H. Huyan, W. Guo, D. Wu, Z. Gu, E. Y. Tsymbal, P. Wang, Y. Nie, and X. Pan, Freestanding crystalline oxide perovskites down to the monolayer limit, *Nature* **570**, 87 (2019).
- [25] G. Kresse and J. Furthmuller, Efficient iterative schemes for ab initio total-energy calculations using a plane-wave basis set, *Phys. Rev. B* **54**, 11169 (1996).
- [26] G. Kresse and J. Furthmuller, Efficiency of ab-initio total energy calculations for metals and semiconductors using a plane-wave basis set, *Computat. Mater. Sci.* **6**, 15 (1996).
- [27] P. Blochl, Projector augmented-wave method, *Phys. Rev. B* **50**, 17953 (1994).
- [28] G. Kresse and D. Joubert, From ultrasoft pseudopotentials to the projector augmented-wave method, *Phys. Rev. B* **59**, 1758 (1999).
- [29] Y. Wang and J. Perdew, Correlation hole of the spin-polarized electron-gas, with exact small-wave-vector and high-density scaling, *Phys. Rev. B* **44**, 13298 (1991).
- [30] S. Dudarev, G. Botton, S. Savrasov, C. Humphreys, and A. Sutton, Electron-energy-loss spectra and the structural stability of nickel oxide: An LSDA+U study, *Phys. Rev. B* **57**, 1505 (1998).
- [31] A. Togo and I. Tanaka, First principles phonon calculations in materials science, *Scripta Mater.* **108**, 1 (2015).
- [32] R. Kingsmith and D. Vanderbilt, Theory of polarization of crystalline solids, *Phys. Rev. B* **47**, 1651 (1993).
- [33] D. Sheppard, P. Xiao, W. Chemelewski, D. D. Johnson, and G. Henkelman, A generalized solid-state nudged elastic band method, *J. Chem. Phys.* **136**, 074103 (2012).
- [34] B. J. Campbell, H. T. Stokes, D. E. Tanner, and D. M. Hatch, *isodisplace*:: a web-based tool for exploring structural distortions, *J. Appl. Cryst.* **39**, 607 (2006).
- [35] N. A. Benedek and C. J. Fennie, Hybrid improper ferroelectricity: A mechanism for controllable polarization-magnetization coupling, *Phys. Rev. Lett.* **106**, 107204 (2011).
- [36] Y.-H. Chu, L. W. Martin, M. B. Holcomb, M. Gajek, S.-J. Han, Q. He, N. Balke, C.-H. Yang, D. Lee, W. Hu, Q. Zhan, P.-L. Yang, A. Fraile-Rodriguez, A. Scholl, S. X. Wang, and R. Ramesh, Electric-field control of local ferromagnetism using a magnetoelectric multiferroic, *Nat. Mater.* **7**, 478 (2008).
- [37] T. Zhao, A. Scholl, F. Zavaliche, K. Lee, M. Barry, A. Doran, M. P. Cruz, Y. H. Chu, C. Ederer, N. A. Spaldin, R. R. Das, D. M. Kim, S. H. Baek, C. B. Eom, and R. Ramesh, Electrical control of antiferromagnetic domains in multiferroic BiFeO_3 films at room temperature, *Nat. Mater.* **5**, 823 (2006).
- [38] J. T. Heron, J. L. Bosse, Q. He, Y. Gao, M. Trassin, L. Ye, J. D. Clarkson, C. Wang, J. Liu, S. Salahuddin, D. C. Ralph, D. G. Schlom, J. Iniguez, B. D. Huey, and R. Ramesh, Deterministic switching of ferromagnetism at room temperature using an electric field, *Nature* **516**, 370-373 (2014).
- [39] S. Li and T. Birol, Suppressing the ferroelectric switching barrier in hybrid improper ferroelectrics, *Npj Comput. Mater.* **6**, 168 (2020).
- [40] E. A. Nowadnick and C. J. Fennie, Domains and ferroelectric switching pathways in $\text{Ca}_3\text{Ti}_2\text{O}_7$ from first principles, *Phys. Rev. B* **94**, 104105 (2016).

- [41] N. Pokhrel and E. A. Nowadnick, Ferroelectric switching pathways and domain structure of $\text{SrBi}_2(\text{Ta,Nb})_2\text{O}_9$ from first principles, *Phys. Rev. B* **107**, 054108 (2023).
- [42] Y. Zhou, S. Dong, C. Shan, K. Ji, and J. Zhang, Two-dimensional ferroelectricity induced by octahedral rotation distortion in perovskite oxides, *Phys. Rev. B* **105**, 075408 (2022).
- [43] K. Inzani, N. Pokhrel, N. Leclerc, Z. Clemens, S. P. Ramkumar, S. M. Griffin, and E. A. Nowadnick, Manipulation of spin orientation via ferroelectric switching in Fe-doped Bi_2WO_6 from first principles, *Phys. Rev. B* **105**, 054434 (2022).
- [44] X.-Z. Lu, H.-M. Zhang, Y. Zhou, T. Zhu, H. Xiang, S. Dong, H. Kageyama, and J. M. Rondinelli, Out-of-plane ferroelectricity and robust magnetoelectricity in quasi-two-dimensional materials, *Sci. Adv.* **9**, eadi0138 (2023).
- [45] T. Zhu, X.-Z. Lu, T. Aoyama, K. Fujita, Y. Nambu, T. Saito, H. Takatsu, T. Kawasaki, T. Terauchi, S. Kurosawa, A. Yamaji, H.-B. Li, C. Tassel, K. Ohgushi, J. M. Rondinelli, and H. Kageyama, Thermal multiferroics in all-inorganic quasi-two-dimensional halide perovskites, *Nat. Mater.* **23**, 182–188 (2024).
- [46] Y. Zhou, Z. Chen, Z. Wu, X. Shen, J. Wang, J. Zhang, and H. Sun, Hybrid improper ferroelectricity and magnetoelectric coupling in a two-dimensional perovskite oxide, *Phys. Rev. B* **103**, 224409 (2021).
- [47] See Supplemental Material for relative energies of phases, mode-resolved analysis, phonon spectra, magnetic anisotropy energy, derivation of $k \cdot p$ model and electronic band structures for 2D-RP structures of $\text{Ca}_3\text{Mn}_2\text{O}_7$, and structural energetics, strain effects, phonon spectra, and magnetic anisotropy energy for the strained 2D-RP structures of $\text{KAg}_2\text{Mn}_2\text{Cl}_7$, which includes Ref. [[74]].
- [48] A. J. Hatt and N. A. Spaldin, Strain effects on the electric polarization of BiMnO_3 , *Eur. Phys. J. B* **71**, 435 (2009).
- [49] N. Sai, C. J. Fennie, and A. A. Demkov, Absence of critical thickness in an ultrathin improper ferroelectric film, *Phys. Rev. Lett.* **102**, 107601 (2009).
- [50] K. F. Garrity, K. M. Rabe, and D. Vanderbilt, Hyperferroelectrics: Proper ferroelectrics with persistent polarization, *Phys. Rev. Lett.* **112**, 127601 (2014).
- [51] H. Akamatsu, K. Fujita, T. Kuge, A. Sen Gupta, A. Togo, S. Lei, F. Xue, G. Stone, J. M. Rondinelli, L.-Q. Chen, I. Tanaka, V. Gopalan, and K. Tanaka, Inversion symmetry breaking by oxygen octahedral rotations in the ruddlesden-popper NaRTiO_4 family, *Phys. Rev. Lett.* **112**, 187602 (2014).
- [52] Z. Guan, H. Hu, X. Shen, P. Xiang, N. Zhong, J. Chu, and C. Duan, Recent progress in two-dimensional ferroelectric materials, *Adv. Electron. Mater.* **6**, 1900818 (2020).
- [53] X.-Y. Ma, H.-Y. Lyu, K.-R. Hao, Y.-M. Zhao, X. Qian, Q.-B. Yan, and G. Su, Large family of two-dimensional ferroelectric metals discovered via machine learning, *Sci. Bull.* **66**, 233 (2021).
- [54] B. H. Chen, T. L. Sun, L. Y. Wei, X. Q. Liu, W. Wen, H. Tian, J. Y. Li, and X. M. Chen, Enhanced hybrid improper ferroelectricity in Fe/Nb cosubstituted $\text{Ca}_3\text{Mn}_2\text{O}_7$ ceramics, *J. Am. Ceram.* **104**, 4000 (2021).
- [55] N. A. Benedek and C. J. Fennie, Hybrid improper ferroelectricity: A mechanism for controllable polarization-magnetization coupling, *Phys. Rev. Lett.* **106**, 107204 (2011).
- [56] M. S. Senn, A. Bombardi, C. A. Murray, C. Vecchini, A. Scherillo, X. Luo, and S. W. Cheong, Negative thermal expansion in hybrid improper ferroelectric ruddlesden-popper perovskites by symmetry trapping, *Phys. Rev. Lett.* **114**, 035701 (2015).
- [57] M. Liu, Y. Zhang, L.-F. Lin, L. Lin, S. Yang, X. Li, Y. Wang, S. Li, Z. Yan, X. Wang, X.-G. Li, S. Dong, and J.-M. Liu, Direct observation of ferroelectricity in $\text{Ca}_3\text{Mn}_2\text{O}_7$ and its prominent light absorption, *Appl. Phys. Lett.* **113**, 022902 (2018).
- [58] L. Šmejkal, J. Sinova, and T. Jungwirth, Emerging research landscape of altermagnetism, *Phys. Rev. X* **12**, 040501 (2022).
- [59] S. Takasuna, J. Shiogai, S. Matsuzaka, M. Kohda, Y. Oyama, and J. Nitta, Weak antilocalization induced by rashba spin-orbit interaction in layered III-VI compound semiconductor gas thin films, *Phys. Rev. B* **96**, 161303 (2017).
- [60] A. D. Caviglia, M. Gabay, S. Gariglio, N. Reyren, C. Cancellieri, and J.-M. Triscone, Tunable rashba spin-orbit interaction at oxide interfaces, *Phys. Rev. Lett.* **104**, 126803 (2010).
- [61] D. Choe, M.-J. Jin, S.-I. Kim, H.-J. Choi, J. Jo, I. Oh, J. Park, H. Jin, H. C. Koo, B.-C. Min, S. Hong, H.-W. Lee, S.-H. Baek, and J.-W. Yoo, Gate-tunable giant non-reciprocal charge transport in noncentrosymmetric oxide interfaces, *Nat. Commun.* **10**, 4510 (2019).
- [62] O. Fedchenko, J. Minár, A. Akashdeep, S. W. D'Souza, D. Vasilyev, O. Tkach, L. Odenbreit, Q. Nguyen, D. Kutnyakhov, N. Wind, L. Wenthaus, M. Scholz, K. Rossnagel, M. Hoesch, M. Aeschlimann, B. Stadtmüller, M. Kläui, G. Schönhense, T. Jungwirth, A. B. Hellenes, G. Jakob, L. Šmejkal, J. Sinova, and H.-J. Elmers, Observation of time-reversal symmetry breaking in the band structure of altermagnetic RuO_2 , *Sci. Adv.* **10**, eadj4883 (2024).
- [63] S. Lee, S. Lee, S. Jung, J. Jung, D. Kim, Y. Lee, B. Seok, J. Kim, B. G. Park, L. Šmejkal, C.-J. Kang, and C. Kim, Broken kramers degeneracy in altermagnetic mnt, *Phys. Rev. Lett.* **132**, 036702 (2024).
- [64] J. C. Wojdeł and J. Íñiguez, Magnetolectric response of multiferroic BiFeO_3 and related materials from first-principles calculations, *Phys. Rev. Lett.* **103**, 267205 (2009).
- [65] G. K. H. Madsen, J. Carrete, and M. J. Verstraete, BoltzTraP2, a program for interpolating band structures and calculating semi-classical transport coefficients, *Comput. Phys. Commun.* **231**, 140 (2018).
- [66] H. Ye, X. Wang, D. Bai, J. Zhang, X. Wu, G. P. Zhang, and J. Wang, Significant enhancement of magnetic anisotropy and conductivity in GaN/CrI_3 van der waals heterostructures via electrostatic doping, *Phys. Rev. B* **104**, 075433 (2021).
- [67] L.-D. Yuan, A. B. Georgescu, and J. M. Rondinelli, Nonrelativistic spin splitting at the brillouin zone center in compensated magnets, *Phys. Rev. Lett.* **133**, 216701 (2024).
- [68] Y. Liu, S.-D. Guo, Y. Li, and C.-C. Liu, Two-dimensional fully compensated ferrimagnetism, *Phys. Rev. Lett.* **134**, 116703 (2025).
- [69] Y.-P. Zhu, X. Chen, X.-R. Liu, Y. Liu, P. Liu, H. Zha, G. Qu, C. Hong, J. Li, Z. Jiang, X.-M. Ma, Y.-J. Hao,

- M.-Y. Zhu, W. Liu, M. Zeng, S. Jayaram, M. Lenger, J. Ding, S. Mo, K. Tanaka, M. Arita, Z. Liu, M. Ye, D. Shen, J. Wrachtrup, Y. Huang, R.-H. He, S. Qiao, Q. Liu, and C. Liu, Observation of plaid-like spin splitting in a noncoplanar antiferromagnet, *Nature* **626**, 523–528 (2024).
- [70] X.-Z. Lu and J. M. Rondinelli, Discovery principles and materials for symmetry-protected persistent spin textures with long spin lifetimes, *Matter* **3**, 1211 (2020).
- [71] H. J. Zhao, H. Nakamura, R. Arras, C. Paillard, P. Chen, J. Gosteau, X. Li, Y. Yang, and L. Bellaiche, Purely cubic spin splittings with persistent spin textures, *Phys. Rev. Lett.* **125**, 216405 (2020).
- [72] J. H. Garcia, M. Vila, C.-H. Hsu, X. Waintal, V. M. Pereira, and S. Roche, Canted persistent spin texture and quantum spin hall effect in WTe_2 , *Phys. Rev. Lett.* **125**, 256603 (2020).
- [73] F. Lou, T. Gu, J. Ji, J. Feng, H. Xiang, and A. Stroppa, Tunable spin textures in polar antiferromagnetic hybrid organic-inorganic perovskites by electric and magnetic fields, *Npj Comput. Mater.* **6**, 114 (2020).
- [74] J. Bardeen, An improved calculation of the energies of metallic Li and Na, *J. Chem. Phys.* **6**, 367 (1938).